Supporting Information

Malhi *et al.* 10.1073/pnas.0804619106

SI Text

Notes on Renormalization Procedure. In an attempt to correct for global climate models (GCM) underesimation of current rainfall, we take the GCM predictions of relative change in monthly rainfall predicted by each GCM but offset these changes to the observed climate for the late 20th century rather than the GCM-simulated climate. For the mean late 21st century, rainfall in month n in GCM i:

$$P_{21}(n, i) = \left(1 + \frac{P_{GCM\_21}(n, i) - P_{GCM\_20}(n, i)}{P_{GCM\_20}(n, i)}\right) \times P_{CRU\_20}(n)$$

where P_{GCM_20} and P_{GCM_21} are GCM-simulated rainfall for the late 20th and 21st centuries, respectively. P_{CRU_20} is the observed monthly climate from the Climate Research Unit (CRU), and P_{21} is the revised estimate of rainfall for the late 21st century. The late 21st-rainfall regime [maximum climatological water deficit (MCWD) and annual precipitation (AP)] is then recalculated from this revised prediction of monthly data, P_{21}, and plotted for E. Amazonia in Fig. 2*B* (and for W. Amazonia in Fig. S3 *Lower*).

This analysis is based on the assumption that GCM simulations better capture future seasonal changes in the relative intensity of precipitation despite their current tendency to underestimate absolute values of precipitation. For two models, P_{GCM_20} is zero or very small, but P_{GCM_21} is non-zero for a few months and, hence, P_{21} is undefined in main text Eq. **1**. For these months (4/228 model months), we limit $P_{\_21}/P_{CRU\_20}$ to a maximum value of 3; variations in this assumption significantly affect the analysis for only one model, IPSL_CM4.

Notes on Vegetation Model Run to Explore Sensitivity of Evapotranspiration to Temperature and Carbon Dioxide. We conducted a sensitivity analysis to explore the effects of changes in temperature and CO_2 concentration on surface evapotranspiration rates, employing the Met Office Surface Exchange Scheme (MOSES) (16). MOSES calculates momentum, heat, vapor, and carbon dioxide exchanges between the land surface and the atmosphere. The model is usually operated at subdaily timescales, typically at 30 min intervals, and at a grid-cell resolution of 3.75° × 2.5°. Transpiration by plants is controlled by canopy conductance, which depends on environmental conditions including soil-moisture status, temperature, humidity, photosynthetically active radiation, atmospheric CO_2 concentration, and plant type (16).

For the current analysis, the most relevant aspects of MOSES are its representation of surface–energy exchange and stomatal conductance. At each timestep, the partitioning of net radiation into evaporative and sensible-heat fluxes is calculated. The modeling of stomatal opening plays a key role in this balance of energy fluxes. In the MOSES model, stomatal conductance is modeled as being nearly linear proportional to net top-leaf-level photosynthesis (i.e., gross primary productivity − dark respiration from leaves) but decreasing with increasing leaf-level humidity deficit. Stomatal conductance is also modeled as decreasing with increasing surface-level atmospheric CO_2 concentration. After these calculations are made, stomatal conductance is then adjusted to take into account soil-moisture status, with stomatal conductance decreasing linearly to zero (i.e., full closure) as leaf-water potentials move between the critical and wilting points. Finally, a canopy-level conductance is calculated, scaling up from leaf-to-canopy following Beer's Law. This final value of stomatal conductance is used in a Penman–Monteith-style energy-balance calculation to determine land-atmosphere vapor and heat fluxes.

Gross Primary Productivity is described as being colimited by temperature and light levels and contains a dependence on internal CO_2 concentration. Dark respiration from leaves has a strong dependence on temperature. Further details may be found in ref. 16.

For the current sensitivity test, in a factorial set of 4 equilibrium experiments, MOSES was run for all 4 combinations of low (preindustrial 286 ppm) and high atmospheric (850ppm) CO_2 concentrations and prescribed temperature increases relative to preindustrial values (26.0 °C) of 0 °C and 4.7 °C across Amazonia. These high CO_2 and temperature values are representative values for the year 2100 for Intergovernmental Panel on Climate Change (IPCC) AR4 Global Climate Models under the A2 emissions scenario (see Fig. S3 and http://www.ipcc.ch/pdf/assessment-report/ar4/syr/ar4_syr.pdf). For these runs, Amazonia is defined as the box −72°W to −48°W, 3°N to 12°S. Precipitation was set at a constant 300 mm/month throughout to ensure the vegetation remained well watered (this high value ensured that all changes in evapotranspiration where mainly driven by surface microclimate and CO_2 rather than seasonal-drought effects). We are exploring potential evapotranspiration rather than actual evapotranspiration. Other surface variables also were consistent with the pattern scaling of the GCM analogue model (17). A fixed, evergreen, broadleaf, forest cover was assumed with upper-temperature threshold for decline of photosynthesis set at 45 °C, a value substantially above the simulated surface temperatures under the high-temperature scenario.

The results of the sensitivity analysis are plotted in Fig. S5. Under preindustrial conditions (CO_2 = 286 ppm, T = 26.0 °C), MOSES simulates an evapotranspiration rate of 3.6 mm/d, close to the 3.33 mm/d that is assumed in our calculation of maximum-water deficit (see main text under *Current Climate and Vegetation in Amazonia*). In the absence of changes in precipitation and with CO_2 concentration kept at preindustrial levels, future warming (ΔT = 4.7 °C) is simulated to increase plant transpiration to 5.7 mm/d across Amazonia. However, simulations suggest a more moderate increase in evapotranspiration of 4.7 mm/d, when stomatal closure at higher ambient CO_2 concentrations (850 ppm) is considered. Finally, high CO_2 alone, without any temperature increase, reduces evapotranspiration to 3.0 mm/d.

In summary, a 4.7 °C increase in surface air temperature (to 30.7 °C), with no change in CO_2 concentration, caused evapotranspiration to rise by 55–57%. A 564 ppm rise in CO_2 (to 850 ppm) caused evapotranspiration to fall by 17–18%. This result suggests that both the temperature and CO_2 effects are of similar order of magnitude, but that the temperature effects are larger by a factor of 3. Hence, potential evapotranspiration rates are likely to increase under 21st century atmospheric change. We emphasise that this analysis is an initial sensitivity test, and the dependency of this result on specific model assumptions warrants deeper exploration.

A major factor determining the relative magnitude of these 2 factors is the relationship between global CO_2 concentrations and regional Amazonian temperatures. If Amazonia warms disproportionately for a given CO_2 concentration, whether

through regional climate factors or local deforestation, the temperature effect may dominate further over the CO_2 effect.

1. Kauffman JB, Uhl C, Cummings DL (1988) Fire in the Venezuelan Amazon. 1. Fuel biomass and fire chemistry in the evergreen rainforest of Venezuela. *Oikos* 53:167–175.
2. Uhl C, Kauffman JB (1990) Deforestation, fire susceptibility, and potential tree responses to fire in the Eastern Amazon. *Ecology* 71:437–449.
3. Kauffman JB (1991) Survival by sprouting following fire in tropical forests of the Eastern Amazon. *Biotropica* 23:219–224.
4. Kauffman JB, Sanford RL, Cummings DL, Salcedo IH, Sampaio E (1993) Biomass and nutrient dynamics associated with slash fires in neotropical dry forests. *Ecology* 74:140–151.
5. Kauffman JB, Cummings DL, Ward DE, Babbitt R (1995) Fire in the Brazilian Amazon. 1. Biomass, nutrient pools, and losses in slashed primary forests. *Oecologia* 104:397–408.
6. Holdsworth AR, Uhl C (1997) Fire in Amazonian selectively logged rain forest and the potential for fire reduction. *Ecol Appl* 7:713–725.
7. Kauffman JB, Cummings DL, Ward DE (1998) Fire in the Brazilian Amazon 2. Biomass, nutrient pools and losses in cattle pastures. *Oecologia* 113:415–427.
8. Alencar A, Nepstad D, Diaz MDV (2006) Forest understory fire in the Brazilian Amazon in ENSO and non-ENSO years: Area burned and committed carbon emissions. *Earth Interact* 10:1–17.
9. Cochrane MA, *et al.* (1999) Positive feedbacks in the fire dynamic of closed canopy tropical forests. *Science* 284:1832–1835.
10. Gerwing JJ (2002) Degradation of forests through logging and fire in the eastern Brazilian Amazon. *Forest Ecol Manage* 157:131–141.
11. Cochrane MA (2003) Fire science for rainforests. *Nature* 421:913–919.
12. Cochrane MA, Laurance WF (2002) Fire as a large-scale edge effect in Amazonian forests. *J Trop Ecol* 18:311–325.
13. Cochrane MA, Schulze MD (1999) Fire as a recurrent event in tropical forests of the eastern Amazon: Effects on forest structure, biomass, and species composition. *Biotropica* 31:2–16.
14. Ray D, Nepstad D, Moutinho P (2005) Micrometeorological and canopy controls of fire susceptibility in a forested Amazon landscape. *Ecol Appl* 15:1664–1678.
15. Barlow J, Peres CA (2008) Fire-mediated dieback and compositional cascade in an Amazonian forest. *Philos Trans R Soc London Ser B* 363:1787–1794.
16. Cox PM, Huntingford C, Harding RJ (1998) A canopy conductance and photosynthesis model for use in a GCM land surface scheme. *J Hydrol* 213:79–94.
17. Huntingford C, *et al.* (2004) Using a GCM analogue model to investigate the potential for Amazonian forest dieback. *Theor Appl Climatol* 78:177–185.
18. Eva HD, *et al.* (2004) A land cover map of South America. *Global Change Biol* 10:731–744.

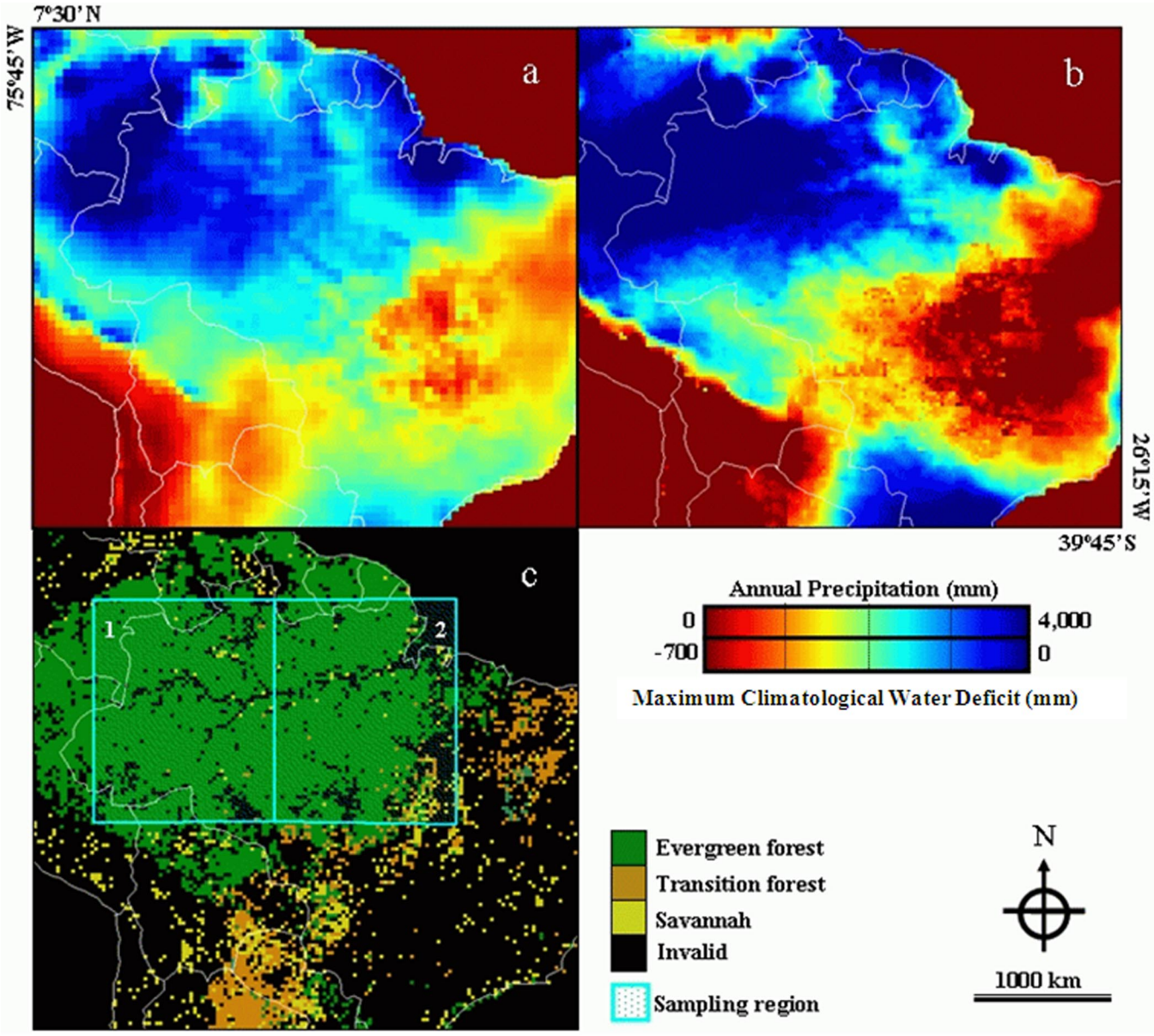

Fig. S1. The variation of rainfall regime and vegetation type across Amazonia, which forms the basis of our biogeographical analysis. Maps of AP (*a*) and CWD (*b*), derived for the period 1998–2007, from the Tropical Rainfall Monitoring Missions (TRMM). (*c*) Map of vegetation cover in 2000, simplified from ref. 18.

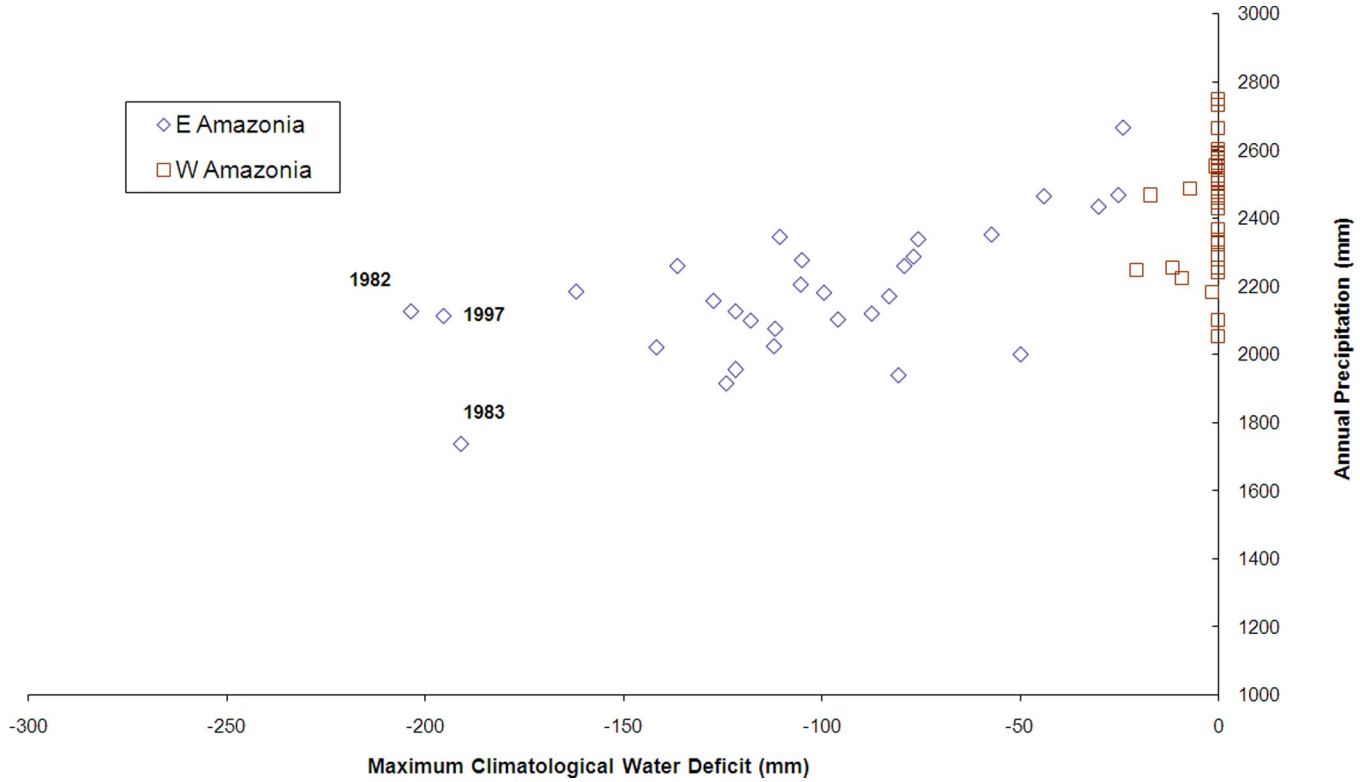

Fig. S2. Interannual variation in rainfall regime in Amazonia, (MCWD and AP). Rainfall values are spatial averages for E. Amazonia (diamonds) and W. Amazonia (squares) for the period 1970–1999. Dry El Niño years are indicated.

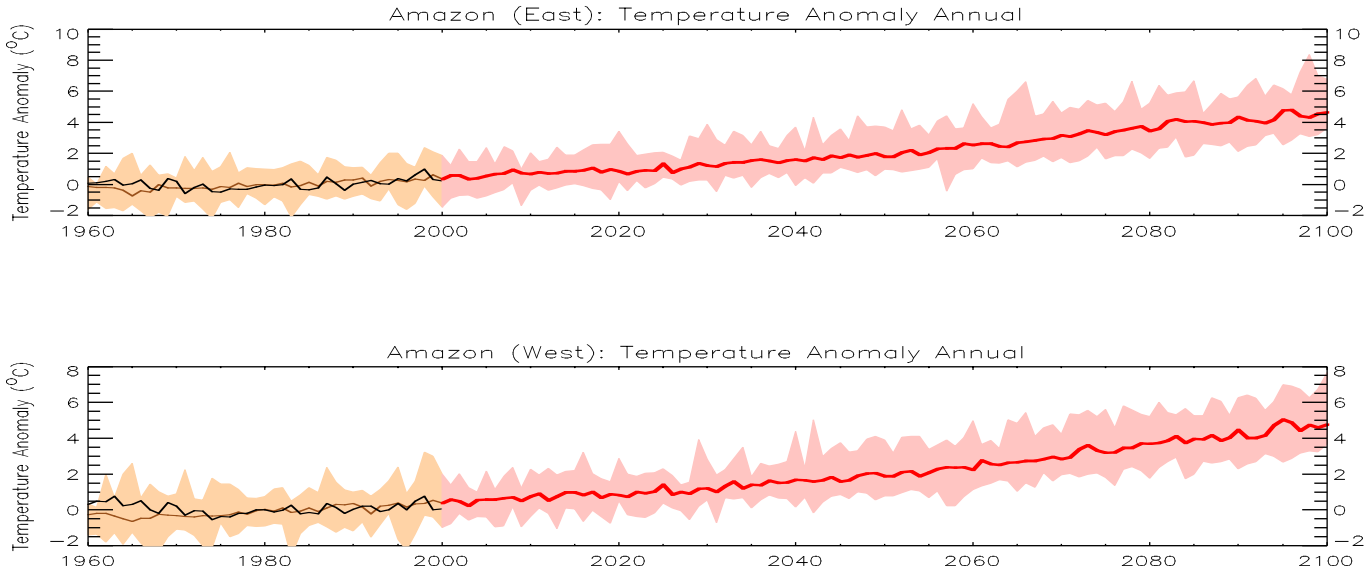

Fig. S3. Observed and projected temperature changes in Amazonia under the IPCC A2 greenhouse gas emissions scenario. Observed and projected mean annual temperature anomalies for E. Amazonia (*Upper*) and W. Amazonia (*Lower*). Observations are from the CRU-interpolated climatology and projections are a mean of the 19 GCMs used in this projection. Models means are indicated by a brown line (observed period) and red line (projections) whereas observations are indicated by the black line. Shaded areas indicate the model range. Anomalies are calculated relative to the period 1970–1999.

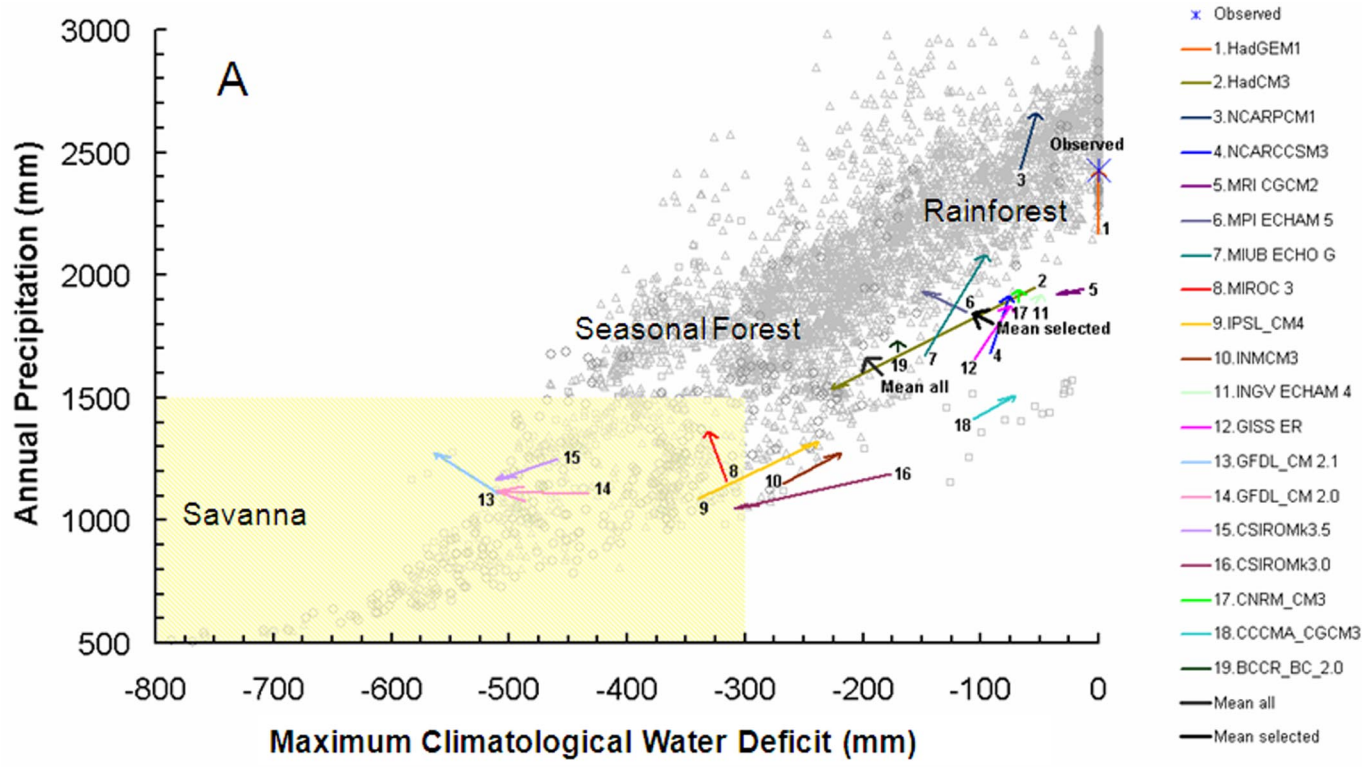

Fig. S4. An evaluation of GCM simulations for change of rainfall regime in W. Amazonia (in contrast to E. Amazonia, which is shown in Fig. 3). (*A*) The rainfall regime simulated by 19 IPCC GCMS for the late 20th century (1970–1999; base of arrow) and projected for the late 21st century (2070–2099; tip of arrow) for the 19 GCMs under the A2 emissions scenario. The TRMM-derived range of rainfall regime in this area is indicated as background gray pixels, the observed CRU climate for 1970–1999 is indicated as a blue star, and the region with a suggested savanna-favouring rainfall regime is shaded. (*B*) The trajectories of changes in GCM rainfall regime when recalculated as relative changes forced to start from the CRU observed climatology. The tip of the arrow indicates the late 21st century rainfall regime.

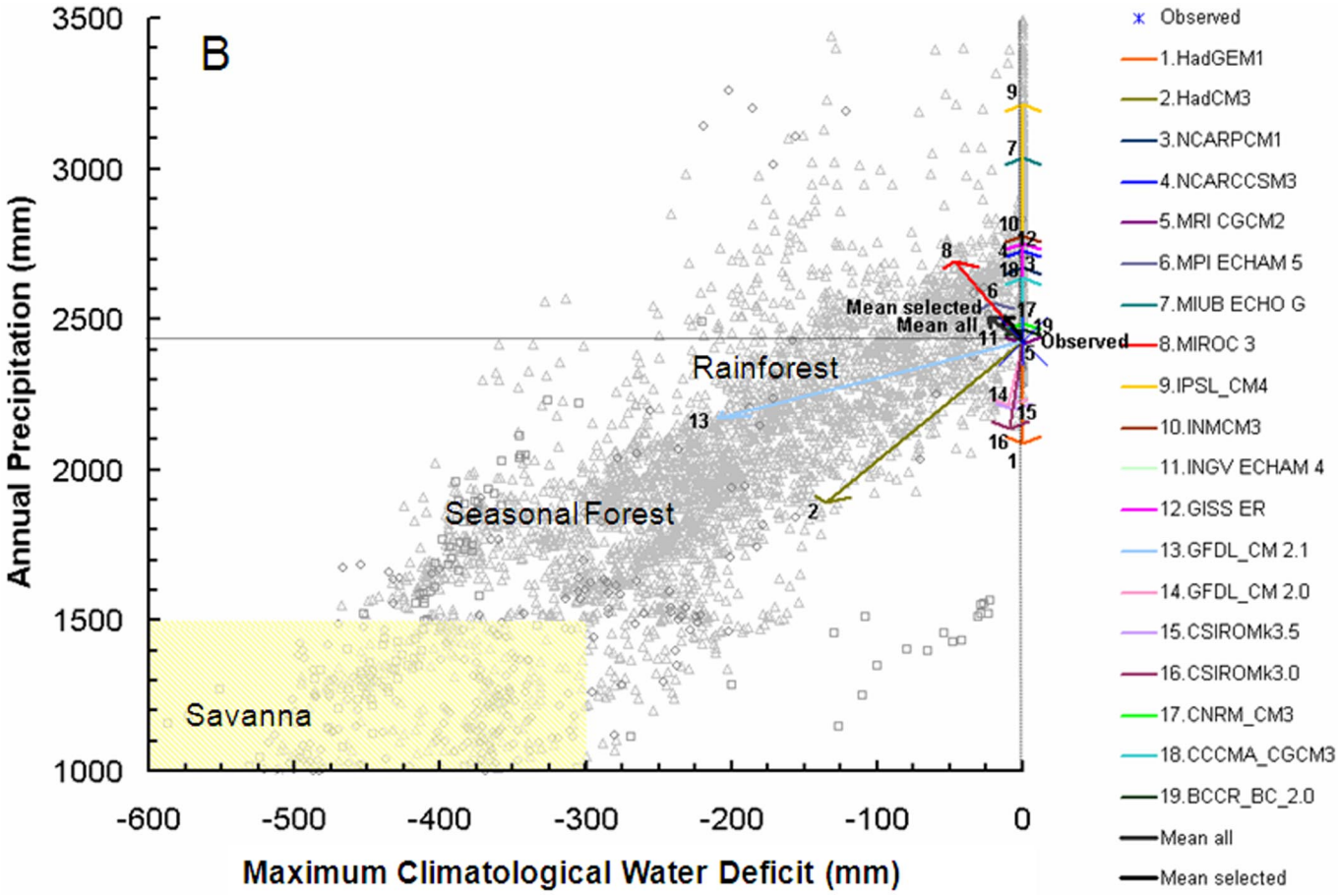

Fig. S4 continued.

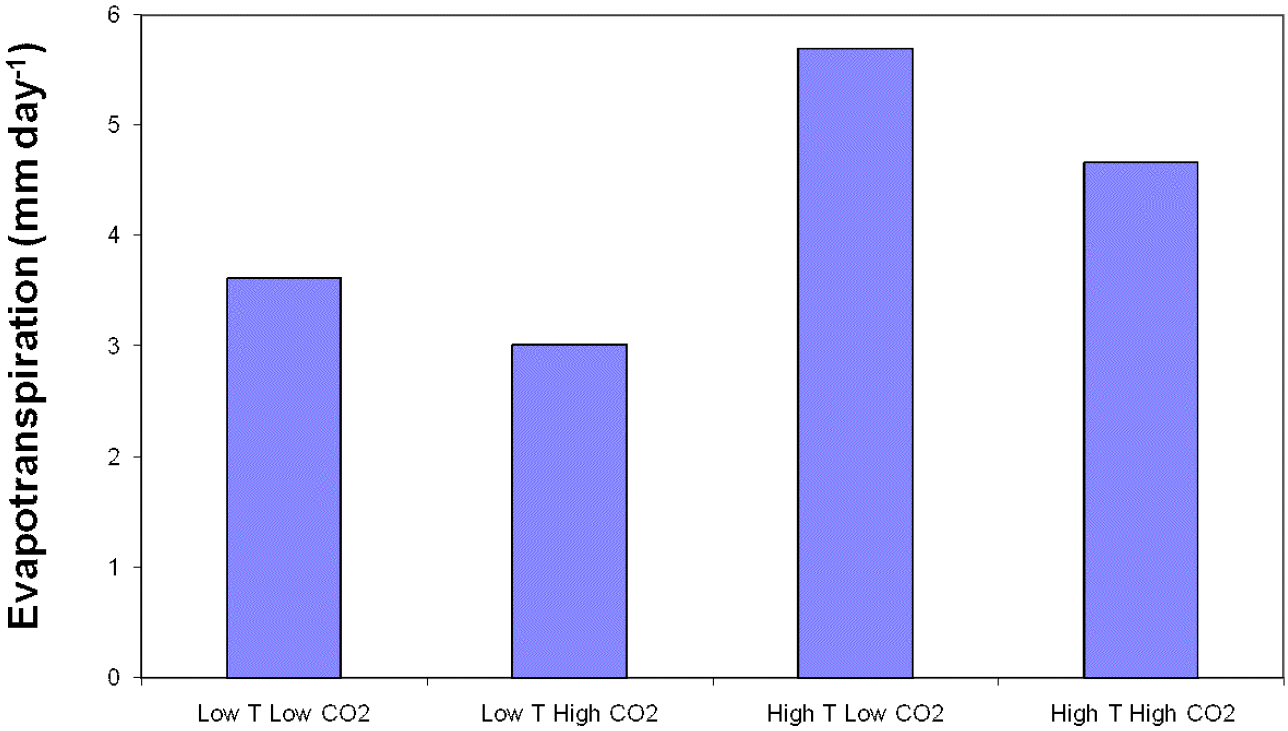

Fig. S5. Results from a factorial-sensitivity analysis of the effects of increased CO_2 and temperature on evapotranspiration rates from evergreen, broadleaf forest. Simulations are for combinations of atmospheric CO_2 (low = 286 ppm; high = 850 ppmv) and Amazonian near-surface air temperature (low = 26.0 °C, high = 30.7 °C; ΔT = 4.7 °C). Low values simulate preindustrial conditions whereas high values are representive of year 2100 values simulated for Amazonia by many GCMs under the A2 greenhouse gas emissions scenario.

Table S1. Summary features of the global climate models used in this analysis

GCM number	GCM Name	Atmospheric Model 1: Name or key reference 2: Resolution 3: Number of vertical levels	Ocean Model 1: Name or key reference 2: Resolution	Land surface Model 1: Name 2: Soil layers 3: Vegetation treatment	Web documentation
1	UKMO-HadGEM1	1: HadGAM1 2: ≈1.3° × 1.9° 3: 38 levels	1: HadGOM1 2: 0.3° − 1.0° × 1.0°	1: MOSES-2 2: 4 soil layers for heat and water 3: Canopy, 5 PFTs	http://www-pcmdi.llnl.gov/ipcc/model_documentation/HadGEM1.htm
2	UKMO-HadCM3	1: HadAM3 2: 2.5° × 3.75° 3: 19 levels	1: HadOM3 2: 1.25° × 1.25°	1: MOSES-1 2: 4 soil layers for heat and water 3: Canopy, 5 PFTs	http://www-pcmdi.llnl.gov/ipcc/model_documentation/HadCM3.htm
3	NCAR-PCM1	1: CCM3 2: ≈2.8° × 2.8° 3: 26 levels	1: POP 2: 0.5° − 0.7° × 1.1°	1: LSM 2: 6 soil layers for heat and water 3: Canopy, 12 PFTs	http://www-pcmdi.llnl.gov/ipcc/model_documentation/PCM.htm
4	NCAR-CCSM3.0	1: CAM3 2: 1.4° × 1.4° 3: 26 levels	1: POP 1.4.3 2: 0.3° − 1.0° × 1.0°	1: CLM3 2: 10 soil layers for heat and water 3: Canopy, 16 PFTs	http://www-pcmdi.llnl.gov/ipcc/model_documentation/CCSM3.htm
5	MRI-CGCM2.3.2	1: MRI/JMA98 2: ≈2.8° × 2.8° 3: 30 levels	1: Bryan-Cox type model 2: 0.5° − 2.0° × 2.5°	1: Based on simple biosphere model 2: 3 soil layers for heat and water 3: Canopy, 13 PFTs	http://www-pcmdi.llnl.gov/ipcc/model_documentation/MRI-GCGM2.3.2.htm
6	MPI-ECHAM5	1: ECHAM5 2: ≈1.9° × 1.9° 3: 19 levels	1: HOPE model (with orthogonal, curvilinear coordinates) 2: 1.5° × 1.5°	1: Hydrological discharge model 2: 5 soil layers for heat and 1 for water 3: Canopy	http://www-pcmdi.llnl.gov/ipcc/model_documentation/ECHAM5_MPI-OM.htm
7	MIUB-ECHO-G	1: ECHAM-4 2: ≈3.9° × 3.9° 3: 19 levels	1: HOPE-G 2: 0.5° − 2.8° × 2.8°	1: Roeckner *et al.* (1) 2: 5 soil layers for heat and 1 for water 3: Canopy	http://www-pcmdi.llnl.gov/ipcc/model_documentation/ECHO-G.htm
8	MIROC 3.2 (medres)	1: AGCM5.7b 2: ≈1.1° × 1.1° 3: 56 levels	1:COCO3.3 2: 0.2° × 0.3°	1: MATSIRO 2: 5 soil layers for heat and 3: Canopy	http://www-pcmdi.llnl.gov/ipcc/model_documentation/MIROC3.2_medres.htm
9	IPSL-CM4	1: LMDZ-4 2: 2.5° × 3.75° 3: 19 levels	1: ORCA 2: 2° × 2°	1: ORCHIDEE 2: 11 soil layers for heat and 2 for moisture 3: Canopy, 12 PFTs	http://www-pcmdi.llnl.gov/ipcc/model_documentation/IPSL-CM4.htm
10	INM-CM3.0	DNM GCM 2: 4.0° × 5.0° 3: 21 levels	1: Diansky *et al.* (2) 2: 2° × 2.5°	1: Dianksy *et al.* (2) 2: 23 soil layers for heat and water 3: Canopy, 13 PFTs	http://www-pcmdi.llnl.gov/ipcc/model_documentation/INM_CM3.0.htm
11	INGV-ECHAM4	1: ECHAM4 2: ≈2.8° × 2.8° 3: 19 levels	1: OPA 8.1 2: 0.5° − 2.0° − 2.0°	None	http://www-pcmdi.llnl.gov/ipcc/model_documentation/INGV-SXG.htm

GCM number	GCM Name	Atmospheric Model 1: Name or key reference 2: Resolution 3: Number of vertical levels	Ocean Model 1: Name or key reference 2: Resolution	Land surface Model 1: Name 2: Soil layers 3: Vegetation treatment	Web documentation
12	GISS-ER	1: GISS Model E 2: 4.0° × 5.0° 3: 20 layers	1: Russell model 2: 4.0° × 5.0°	1: Friend and Kiang (3) 2: 6 soil layers for heat and water 3: Canopy, 8 PFTs	http://www-pcmdi.llnl.gov/ipcc/model_documentation/GISS-E.htm
13	GFDL-CM2.1	1: AM2P13 2: 2.0° × 2.5° 3: 24 levels	1: OM3P4 2: 0.3° − 1.0° × 1.0°	1: LM2 2: 18 soil layers for heat and water 3: Canopy, 8 PFTs	http://www-pcmdi.llnl.gov/ipcc/model_documentation/GFDL-cm2.htm
14	GFDL-CM2.0	1: AM2P13 2: 2.0° × 2.5° 3: 24 levels	1: OM3P4 2: 0.3° − 1.0° × 1.0°	1: LM2 2: 18 soil layers for heat and water 3: Canopy, 8 PFTs	http://www-pcmdi.llnl.gov/ipcc/model_documentation/GFDL-cm2.htm
15	CSIRO-MK3.5	1: mk3 AGCM 2: ≈1.9° × 1.9° 3: 18 levels	1: MOM2.2 2: 0.8° × 1.9°	1: Gordon *et al.* (4) 2: 6 soil layers for heat and water 3: Canopy, 11 PFTs	http://www-pcmdi.llnl.gov/ipcc/model_documentation/CSIRO-Mk3.5.htm
16	CSIRO-MK3.0	1: mk3 AGCM 2: ≈1.9 × 1.9 3: 18 levels	1: MOM2.2 2: 0.8° × 1.9°	1: Gordon *et al.* (4) 2: 6 soil layers for heat and water 3: Canopy, 11 PFTs	http://www-pcmdi.llnl.gov/ipcc/model_documentation/CSIRO-Mk3.0.htm
17	CNRM-CM3	1: ARPEGE-Climat and 2: v.3 ≈1.9° × 1.9° 3: 45 levels	1: OPA8.1 2: 0.5° − 2.0° × 2°	1: ISBA 2: 4 soil layers for heat and 2 for water 3: ECOCLIMAP vegetation and phenology	http://www-pcmdi.llnl.gov/ipcc/model_documentation/CNRM-CM3.htm
18	CCCMA-CGCM3.1	1: AGCM3 2: ≈2.8° × 2.8° 3: 29 levels	1: Flato and Boer (5) 2: 1.9° × 1.9°	1: CLASS 2: 3 soil layers for heat and water 3: Canopy	http://www.cccma.bc.ec.gc.ca/models/cgcm3.shtml
19	BCCR-BCM2.0	1: ARPEGE-Climat Version 3 2: 1.9° × 1.9° 3: 31 levels	1: NERSC-modified version of MICOM v. 2.8 2: 0.5° − 1.5° × 1.5°	1: ISBA 2: 4 soil layers for heat and 2 for water 3: ECOCLIMAP vegetation and phenology	http://www-pcmdi.llnl.gov/ipcc/model_documentation/BCCR_BCM2.0.htm

1. Roeckner EK, *et al*. (1996) The atmospheric general circulation model ECHAM-4: Model description and simulation of present-day climate (Reports of the Max-Planch-Institute, Hamburg, no. 218).
2. Diansky NA, *et al*. (2002) Sigma model of global ocean circulation and its sensitivity to variations in wind stress. *Izv Atmos Ocean Phys* (Engl. Transl.), 38:477–494.
3. Friend AD, Kiang NY (2005) Land surface model development for the GISS GCM: Effects of improved canopy physiology on simulated climate. *J Climate* 18:2883–2902.
4. Gordon HB, *et al*. (2002) The CSIRO Mk3 Climate System Model (CSIRO Atmospheric Research technical paper, no. 60).
5. Flato GM, Boer GJ (2001) Warming asymmetry in climate change simulations. *Geophys Res Lett* 28:195–198.

Table S2. The rainfall regime (mean AP and CWD) of the global models used in this analysis in E. and W. Amazonia in the late 20th century (1970–1999) and late 21st century (2070–2099)

GCM number	GCM institute/name	W. Amazonia late 20th century mean annual rainfall regime, mm/yr	W. Amazonia late 21st century mean annual rainfall regime, mm/yr	W. Amazonia late 21st century CRU-adjusted rainfall regime, mm/yr	E. Amazonia late 20th century mean annual rainfall regime, mm/yr	E. Amazonia late 21st century mean annual rainfall regime, mm/yr	E. Amazonia late 21st century CRU-adjusted rainfall regime, mm/yr
1	UKMO-HadGEM1	Precip: 2169.42 CWD: 0.00	Precip: 1912.00 CWD: 0.00	Precip: 2088.96 CWD: 0.00	Precip: 1667.30 CWD: −271.86	Precip: 1260.32 CWD: −368.70	Precip: 1604.36 CWD: −268.07
2	UKMO-HadCM3	Precip: 1948.70 CWD: −53.79	Precip: 1532.95 CWD: −227.39	Precip: 1891.28 CWD: −135.47	Precip: 1144.65 CWD: −414.41	Precip: 653.55 CWD: −634.81	Precip: 1156.71 CWD: −493.21
3	NCAR-PCM1	Precip: 2431.44 CWD: −69.86	Precip: 2661.57 CWD: −52.54	Precip: 2672.40 CWD: 0.00	Precip: 902.80 CWD: −690.71	Precip: 1008.62 CWD: −488.63	Precip: 2456.79 CWD: −94.89
4	NCAR-CCSM3.0	Precip: 1679.27 CWD: −95.47	Precip: 1913.93 CWD: −76.31	Precip: 2727.16 CWD: 0.00	Precip: 1492.90 CWD: −166.33	Precip: 1594.38 CWD: −174.49	Precip: 2359.87 CWD: −108.94
5	MRI-CGCM2.3.2	Precip: 1945.86 CWD: −16.52	Precip: 1917.81 CWD: −36.28	Precip: 2418.54 CWD: 0.00	Precip: 1815.25 CWD: 0.00	Precip: 1795.23 CWD: −50.48	Precip: 2235.14 CWD: −139.04
6	MPI-ECHAM5	Precip: 1850.25 CWD: −115.20	Precip: 1937.44 CWD: −149.53	Precip: 2555.42 CWD: −21.70	Precip: 942.75 CWD: −471.36	Precip: 894.11 CWD: −527.91	Precip: 1890.68 CWD: −390.85
7	MIUB-ECHO-G	Precip: 1673.75 CWD: −151.54	Precip: 2084.09 CWD: −95.54	Precip: 3035.41 CWD: 0.00	Precip: 1487.34 CWD: −246.00	Precip: 1484.17 CWD: −337.61	Precip: 2140.26 CWD: −248.67
8	MIROC 3.2 (medres)	Precip: 1161.71 CWD: −322.48	Precip: 1361.94 CWD: −331.12	Precip: 2691.11 CWD: −46.89	Precip: 1420.57 CWD: −422.13	Precip: 1315.37 CWD: −451.13	Precip: 1870.59 CWD: −287.96
9	IPSL-CM4	Precip: 1087.36 CWD: −349.30	Precip: 1321.94 CWD: −237.05	Precip: 3212.63 CWD: 0.00	Precip: 751.68 CWD: −598.22	Precip: 977.28 CWD: −459.81	Precip: 3284.17 CWD: −24.19
10	INM-CM3.0	Precip: 1151.01 CWD: −274.57	Precip: 1276.47 CWD: −218.06	Precip: 2776.80 CWD: 0.00	Precip: 937.93 CWD: −580.05	Precip: 907.29 CWD: −546.89	Precip: 2123.34 CWD: −230.41
11	INGV-ECHAM4	Precip: 1882.62 CWD: −54.30	Precip: 1921.84 CWD: −48.36	Precip: 2486.98 CWD: 0.00	Precip: 1125.53 CWD: −344.05	Precip: 1059.37 CWD: −415.94	Precip: 2016.61 CWD: −242.65
12	GISS-ER	Precip: 1654.65 CWD: −109.21	Precip: 1875.85 CWD: −75.29	Precip: 2752.75 CWD: 0.00	Precip: 1962.21 CWD: −106.75	Precip: 2114.10 CWD: −78.89	Precip: 2342.26 CWD: −79.46
13	GFDL-CM2.1	Precip: 1110.08 CWD: −519.19	Precip: 1275.22 CWD: −563.19	Precip: 2172.72 CWD: −209.84	Precip: 1067.16 CWD: −582.97	Precip: 1046.58 CWD: −600.20	Precip: 1809.97 CWD: −404.58
14	GFDL-CM2.0	Precip: 1110.33 CWD: −442.58	Precip: 1117.51 CWD: −511.12	Precip: 2213.09 CWD: −10.04	Precip: 1118.38 CWD: −614.63	Precip: 1017.20 CWD: −636.65	Precip: 2024.02 CWD: −210.38
15	CSIRO-MK3.5	Precip: 1251.52 CWD: −469.26	Precip: 1163.90 CWD: −511.92	Precip: 2199.00 CWD: −6.50	Precip: 648.80 CWD: −729.77	Precip: 597.85 CWD: −760.18	Precip: 1784.59 CWD: −244.16
16	CSIRO-MK3.0	Precip: 1192.18 CWD: −195.40	Precip: 1047.95 CWD: −308.84	Precip: 2138.45 CWD: −9.29	Precip: 747.63 CWD: −518.80	Precip: 743.74 CWD: −532.94	Precip: 2072.78 CWD: −187.81
17	CNRM-CM3	Precip: 1890.95 CWD: −67.53	Precip: 1941.80 CWD: −67.73	Precip: 2485.93 CWD: 0.00	Precip: 1501.71 CWD: −204.70	Precip: 1623.76 CWD: −193.69	Precip: 2318.01 CWD: −93.89
18	CCCMA-CGCM3.1	Precip: 1410.67 CWD: −110.01	Precip: 1506.92 CWD: −70.56	Precip: 2637.46 CWD: 0.00	Precip: 900.70 CWD: −408.46	Precip: 823.05 CWD: −434.47	Precip: 2013.42 CWD: −157.37
19	BCCR-BCM2.0	Precip: 1688.50 CWD: −173.33	Precip: 1729.81 CWD: −170.82	Precip: 2468.68 CWD: 0.00	Precip: 1197.72 CWD: −354.18	Precip: 1372.50 CWD: −317.15	Precip: 2540.76 CWD: −56.11

Table S3. A selection of reported studies of fires in Amazonian forests

No.	Location	References	Latitude	Longitude	Type
1	Near the confluence of the Casiquiare River and the Rio Negro	1	−1.93	−67.05	Observation
2	6.5 km northwest of Paragominas	2	−2.92	−47.57	Observation
3	Itaruman, Berrante, Pimental, and Vitoria (near Paragominas)	3	−2.92	−47.57	Observation
4	Serra Talhada research station, Pernambuco	4	−7.98	−38.32	Observation
5	Nova Jacunda, Para	5	−4.05	−49	Observation
6	Maraba, Para	5	−5.37	−49.12	Observation
7	Santa Barbara and Jamari, Rondonia	5	−9.2	−60.05	Observation
8	Fazenda Vitoria, Fazenda Sete (near Paragominas)	6	−2.92	−47.57	Observation
9	Near Maraba, Para	7	−5.35	−49.15	Observation
10	Near Jamari, Rondonia	7	−9.2	−60.05	Observation
11	Paragominas, Para	8–10	−3	−47.35	Observation
12	Tailandia, Para	9, 11, 12	−2.94	−48.94	Observation
13	Santana do Araguaia, South of Para	8, 9	−9.3	−50.1	Observation
14	Alta Floresta, Mato Grosso	8, 9	−9.9	−55.9	Observation
15	Olho d'Agua, Para	13	−12.02	−44.03	Observation
16	100 km South from Santarem, Para	14	−38	−55	Experiment
17	Rio Maro (westernmost Para)	15	−2.73	−55.68	Observation